Luminescent fac-[ReX(CO)3(phenyl-pyta)] (X = Cl, Br, I) complexes: influence of the halide ligand on the electronic properties in solution and in the solid state

Alexandre Poirot, Corinne Vanucci-Bacqué, Béatrice Delavaux-Nicot, Nathalie Saffon-Merceron, Charles-Louis Serpentini, Nadine Leygue, Florence Bedos-Belval, Eric Benoist, Suzanne Fery-Forgues

Luminescent *fac*-[ReX(CO)$_3$(phenyl-pyta)] (X = Cl, Br, I) complexes: Influence of the halide ligand on the electronic properties in solution and in the solid state

Alexandre Poirot[1], Corinne Vanucci-Bacqué[1], Béatrice Delavaux-Nicot [2], Nathalie Saffon-Merceron[3], Charles-Louis Serpentini[4], Nadine Leygue[1], Florence Bedos-Belval[1], Eric Benoist[1], Suzanne Fery-Forgues[1*]

1 *SPCMIB, CNRS UMR 5068, Université de Toulouse III Paul Sabatier, 118 route de Narbonne, 31062 Toulouse cedex 9, France. *E-mail: suzanne.fery-forgues@univ-tlse3.fr*

2 *Laboratoire de Chimie de Coordination du CNRS (LCC), CNRS UPR 8241, 205 route de Narbonne, Université de Toulouse, 31077 Toulouse Cedex 4, France*

3 *Service Diffraction des Rayons X, Institut de Chimie de Toulouse, ICT- UAR 2599, Université de Toulouse III Paul Sabatier, 118 route de Narbonne, 31062 Toulouse cedex 9, France*

4 *Laboratoire IMRCP, CNRS UMR 5623, Université de Toulouse III Paul Sabatier, 118 route de Narbonne, 31062 Toulouse cedex 9, France*

† Electronic Supplementary Information (ESI) available: Experimental details including proton numbering for NMR, NMR spectra, molecular views and crystallographic data, additional computational and electrochemical data, fluorescence microscopy images.

Abstract

Tricarbonylrhenium(I) complexes that incorporate a chloride ligand are promising photoluminescent materials, but those incorporating a bromide or iodide ligand have received very little attention regarding their solid-state properties. In this work, three rhenium(I) complexes differing only by the nature of their halide ligand (X = Cl, Br, and I) were compared. They are based on a *fac*-[ReX(CO)$_3$(N^N)] framework where the N^N bidentate ligand is a 3-(2-pyridyl)-1,2,4-triazole unit functionalized by an appended phenyl group. DFT calculations showed that the character of the lowest energy transitions progressively changes from Re → N^N ligand (MLCT) to X → N^N ligand (XLCT) when increasing the size of the halogen atom. Regarding the electrochemical behavior, the chloride and bromide complexes **1-Cl** and **1-Br** were similar, while the iodide complex **1-I** exhibited a strikingly different electrochemical signature in oxidation. From a spectroscopic viewpoint, all three complexes emitted weak red-orange phosphorescence in dichloromethane solution. However, in the solid state, marked differences appeared. Not only was **1-Cl** a good emitter of yellow light, but it had strong solid-state luminescence enhancement (SLE) properties. In comparison, **1-Br** and **1-I** were less emissive and they showed better mechanoresponsive luminescence (MRL) properties, probably related to a loose molecular arrangement in the crystal packing and to the opening of vibrational non-radiative deactivation pathways. This study highlights for the first time how the nature of the halide ligand in this type of complex allows fine tuning of the solid-state optical properties, for potential applications either in bio-imaging or in the field of MRL-active materials.

Keywords Rhenium · Photoluminescence · Crystal · DFT · Electrochemistry · Halogen

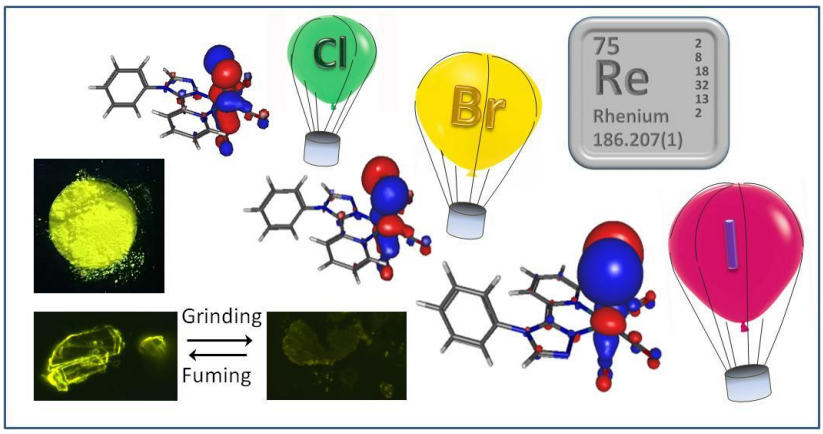

1 Introduction

Since the discovery of their photoluminescence properties in 1974, the air- and moisture-stable tricarbonyl rhenium(I) complexes have attracted considerable attention for applications as bioimaging agents [1, 2]. The interest that they generate as solid-state light emitters is much more recent. They are now being considered for applications in the fields of electroluminescence [3, 4], solar energy conversion [5, 6], photocatalysis [7], and smart materials with thermochromic [8], photochromic [9] and mechanical strength sensing [10] abilities. These complexes usually incorporate a bidentate organic ligand and an ancillary ligand that can be organic or inorganic. The nature of both ligands totally governs the optical properties and photochemical stability. It is generally considered that the presence of a chloride anion as ancillary ligand leads to superior photochemical stability. Bromide tricarbonyl rhenium(I) complexes have also been studied for their spectroscopic and photophysical properties in solution [11–20], in polymer films [20], and for use as potential luminophores for bioimaging [21–23]. Some of them have also been investigated for their capacity to act as photochemically CO-releasing molecules (PhotoCORMs) [24, 25]. Iodide complexes are much rarer, probably because their synthesis is more demanding and because poor stability may be feared. However, some stable luminescent tricarbonylrhenium(I) complexes incorporating an iodide ligand have been reported in the literature, one of them being the first example in this series of compounds to exhibit circularly polarized phosphorescence [26]. Using a coupled theoretical and experimental approach, the teams of Vlček and Daniel have thoroughly studied the photophysical properties of the three isologs of $[ReX(CO)_3(bipyridine)]$ with X = Cl, Br and I, thus revealing that the nature of the halide ligand determines the excited state character of the complexes in fluid solution. [27–32]. Regarding the solid-state properties, the aggregation-induced phosphorescence emission enhancement (AIPE) of bromide complexes has recently been reported [33] as well as the integration of such complexes in phosphorescent organic light-emitting diodes (OLEDs) [3, 34, 35]. Finally, the behavior of three isologs adsorbed on a TiO_2 semiconductor has been compared, showing that the iodide complex performed better as a sensitizer for solar energy conversion [5]. However, it is not clear how the nature of the halide ligand influences the spectroscopic solid-state properties of these complexes. On the one hand, a direct electronic effect may be expected since the ligand field strengths for the halogen ligands related to dd transitions increases in the order: $I^- < Br^- < Cl^-$ [5]. On the other hand, it has been well established in the field of organic compounds that the nature of the halogen has a strong impact upon the crystal packing mode, and hence upon the emission behavior that is closely linked to the molecular arrangement [36–39]. It would be instructive to know how these two effects are combined for tricarbonylrhenium(I) complexes.

In the last few years, our group has introduced new mononuclear tricarbonyl rhenium(I) complexes [40] the most promising of which are based on a 3-(2-pyridyl)-1,2,4-triazole (pyta) bidentate ligand bearing a phenyl ring on the 4-position [41]. Complex **1-Cl** (Fig. 1) is the simplest member of this series [42]. Substituting the phenyl group in the *para* position by a benzoxazole moiety [10, 41] or aliphatic bulky groups [42] allowed access to more elaborate molecules. All these molecules show excellent photoluminescence (PL) properties in the solid state, with strong solid-state luminescence enhancement (SLE) behavior, *i.e.* the rare property to be much more emissive in the solid state than in solution, which makes them very attractive candidates for aggregation studies and applications in the field of optical materials. The synthesis of complex **1-Cl** has been recently optimized [42], so we have embarked on the preparation of the bromide (**1-Br**) and iodide (**1-I**) complexes (Fig. 1), with the aim to make a systematic comparison between three analogs differing only by the halogen atom. It is therefore shown that the nature of the halide ligand considerably influences the solid state properties and must be taken into account when selecting a complex for a given application.

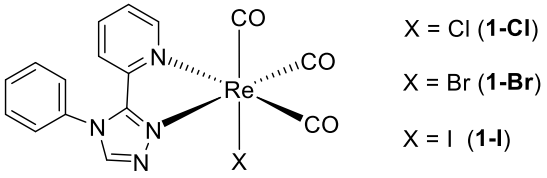

Fig. 1 Chemical structure of the tricarbonyl rhenium(I) complexes

2 Experimental section

2.1 Materials and methods

All purchased chemicals were of the highest purity commercially available and used without further purification. Analytical grade solvents were used as received. Experiments were carried out under a nitrogen atmosphere. Reactions were monitored by TLC on silica gel Alugram® Xtra SIL G/UV_{254}. Column chromatography was performed on Machery-Nagel silica gel or neutral alumina.

NMR, mass and infrared spectra were obtained in the relevant 'Services communs de l'Institut de Chimie de Toulouse, Université de Toulouse III-Paul-Sabatier'. ^{1}H- and ^{13}C-NMR spectra were recorded on a Bruker Avance 300 MHz spectrometer. Attributions of the signals were made using 2D NMR data (COSY, HSQC and HMBC). Protons and carbon atoms were numbered according to Fig. S1† ESI. Signals are described as follow: s, singlet; d, doublet; t, triplet; m, multiplet. HRMS data were recorded on a Xevo G2 QTOF (Waters) instrument. Infrared spectra were obtained on a Nexus Thermonicolet apparatus with DTGS as the detector.

2.2 Synthesis

The synthesis of ligand 2-(4-phenyl-*4H*-1,2,4-triazol-3-yl)pyridine **(L1)** and complex **[ReCl(CO)$_3$(L1)]** (**1-Cl**) has been previously described [42].

Complex [ReBr(CO)$_3$(L1)], 1-Br. A mixture of ligand **L1** (21.5 mg, 0.096 mmol) and [ReBr(CO)$_5$] (41 mg, 0.101 mmol) in methanol (5 mL) was stirred for 16 h at 65 °C. The reaction mixture was cooled to room temperature and the yellow precipitate was collected by filtration, washed with methanol and dried *in vacuo* (38.8 mg, 70 %). The expected complex **1-Br** was pure enough to be used without further purification.

^{1}H NMR (300 MHz, $CDCl_3$): δ (ppm) = 9.15 (ddd, *J* = 5.5, 1.6, 0.9 Hz, 1H, H_1), 8.34 (s, 1H, H_7), 7.81–7.70 (m, 4H, $H_{3\text{-}10\text{-}11}$); 7.59–7.54 (m, 2H, H_9); 7.49 (ddd, *J* = 7.8, 5.5, 1.3 Hz, 1H, H_2); 7.05 (dt, *J* = 8.1, 1.1 Hz, 1H, H_4).^{13}C NMR (75 MHz, $CDCl_3$): δ (ppm) = 196.9; 195.1; 187.8; 155.1; 154.5; 146.5; 144.9; 138.8; 132.4; 132.2; 131.3; 127.5; 126.4; 122.8. HRMS (ESI) *m/z* 594.9380 ([M+Na]$^+$ calcd for $C_{16}H_{10}N_4O_3NaBr^{185}Re$: 594.9391). IR ($CH_2Cl_2$): ν(CO) = 2028, 1928, 1900 cm^{-1}. IR (KBr): ν(CO) = 2021, 1914, 1880 cm^{-1}. Anal. calcd (%) for $C_{16}H_{10}N_4O_3ReBr$: C 33.57, H 1.76, N 9.79; found: C 34.34, H 1.73, N 9.23.

Complex [ReI(CO)$_3$(L1)], 1-I. The complex [ReI(CO)$_5$] was prepared by reacting dirhenium decacarbonyl with diodide in CCl_4 and purified by sublimation [43]. Then a mixture of ligand **L1** (91 mg, 0.41 mmol) and [ReI(CO)$_5$] (194.5 mg, 0.43 mmol) in methanol (5 mL) was stirred for 16 h at 65 °C. The solvent was removed *in vacuo* and the crude product was purified by column chromatography on silica gel (CH_2Cl_2) to provide complex **1-I** (83 mg, 33%) as a yellow solid.

^{1}H NMR (300 MHz, $CDCl_3$): δ (ppm) = 9.20 (ddd, *J* = 5.5, 1.6, 0.9 Hz, 1H, H_1), 8.35 (s, 1H, H_7), 7.82–7.70 (m, 4H, $H_{3\text{-}10\text{-}11}$); 7.59–7.52 (m, 2H, H_9); 7.46 (ddd, *J* = 7.8, 5.5, 1.3 Hz, 1H, H_2); 7.05 (ddd, *J* = 8.1, 1.3 ,0.8 Hz, 1H, H_4). ^{13}C NMR (75 MHz, DMSO- d_6): δ (ppm) = 196.5; 196.2; 187.8; 155.1; 153.9; 148.3; 144.2; 140.3; 132.2; 131.6; 130.7; 128.0; 126.9; 122.9. HRMS (ESI) *m/z* 640.9243 ([M+Na]$^+$ calcd for $C_{16}H_{10}N_4O_3NaI^{185}Re$: 640.9225). IR ($CH_2Cl_2$): ν(CO) = 2027, 1930, 1903 cm^{-1}. IR (KBr): ν(CO) = 2023, 1916, 1885 cm^{-1}. Anal. calcd (%) for $C_{16}H_{10}N_4O_3ReI$: C 31.03, H 1.63, N 9.05; found: C 31.06, H 1.51, N 8.25.

2.3 Crystallography

Crystal data were collected at 193K using MoKα radiation (wavelength = 0.71073 Å) on a Bruker AXS Quazar APEX II diffractometer using a 30 W air-cooled microfocus source (ImS) with focusing multilayer optics. Phi- and omega-scans were used. Space group was determined on the basis of systematic absences and intensity statistics. Semi-empirical absorption correction was employed [44]. The structures were solved using an intrinsic phasing method (ShelXT) [45]. All non-hydrogen atoms were refined anisotropically using the least-square method on F^2 [46]. Hydrogen atoms were refined isotropically at calculated positions using a riding model with their isotropic displacement parameters constrained to be equal to 1.5 times the equivalent isotropic displacement parameters of their pivot atoms for terminal sp3 carbon and 1.2 times for all other carbon atoms. In both structures, the solvent (chloroform) was disordered over two positions. Several restraints (SAME, SIMU, DELU) were applied to refine some moieties of the molecules and to avoid the collapse of the structures during the least-squares refinement by the large anisotropic displacement parameters. In both structures, the halogen atom and the CO group *trans* to it were disordered, so that the restraints SAME, SIMU, DELU, ISOR and FLAT were applied. Some bond lengths were restrained with DFIX to suitable target values (1-I). Selected crystallographic data are collected in Table 1.

Table 1 Selected crystallographic data of complexes **1-Br** and **1-I**.

	1-Br	**1-I**
Empirical formula	$C_{16}H_{10}BrN_4O_3Re$, ½ $CHCl_3$	$C_{16}H_{10}IN_4O_3Re$, ½ $CHCl_3$
Formula weight	632.07	679.06
Crystal system	Triclinic	Triclinic
Space group	$P\ \bar{1}$	$P\ \bar{1}$
Unit cell dimensions		
a (Å)	11.5342(11)	11.7786(7)
b (Å)	11.9767(10)	12.0288(6)
c (Å)	13.8827(13)	14.1724(7)
α (°)	99.941(3)	100.6633(17)
β (°)	93.927(3)	94.0925(17)
γ (°)	93.362(3)	93.4501(17)
Volume ($Å^3$)	1879.7(3)	1962.75(18)
Z	4	4
Density (calculated) (Mg/m^3)	2.234	2.298
Crystal size (mm^3)	0.120 × 0.040 × 0.020	0.160 × 0.080 × 0.030
Reflections collected	42207	68421
Independent reflections	7519	9876
R_{int}	0.0742	0.0708
Restraints/parameters	188/580	215/560
Final R1 index I>2σ(I)	0.0381	0.0419
wR2 (all data)	0.0683	0.1124
Largest diff. peak and hole (e $Å^{-3}$)	0.941 and -1.285	1.366 and -2.335
CCDC	2089472	2167320

2.4 Electrochemistry

The electrochemical properties of the new compounds were determined by cyclic voltammetry (CV) and Osteryoung square wave voltammetry (OSWV) in DCM. The solutions used during the electrochemical studies were typically 1×10^{-3} M in complex, and 0.1 M in supporting electrolyte. The supporting electrolyte [*n*Bu_4N][BF_4] (Fluka, 99% electrochemical grade) was used as received and simply degassed under Ar. DCM was dried using an MB SPS-800 solvent purification system just prior to use. The measurements were carried out with an Autolab PGSTAT100 potentiostat controlled by GPES 4.09 software. Experiments were performed at room temperature (r.t.) in a homemade airtight three-electrode cell connected to a vacuum/Ar line. The reference electrode consisted of a saturated calomel electrode (SCE) separated from

the solution by a bridge compartment. The counter electrode was a Pt wire of ca. 1 cm^2 apparent surface. The working electrode was a Pt microdisk (0.5 mm diameter). Before each measurement, the solutions were degassed by bubbling Ar and the working electrode was polished with a polishing machine (Presi P230). Under these experimental conditions, Fc^+/Fc is observed at +0.55 ± 0.01 V *vs*. SCE. OSWVs were obtained using an amplitude of 20 mV, a frequency of 20 Hz, and a step potential of 5 mV.

2.5 Spectroscopy

When not specified, undegassed solutions were used. Deaerated solutions where bubbled with argon for 5 min. Spectroscopic measurements in solutions were conducted at 20°C in a temperature-controlled cell. UV-visible absorption spectra and emission spectra in solutions were measured with a Xenius SAFAS spectrofluorometer using cells of 1 cm optical pathway. All emission spectra were corrected. The emission quantum yields in solution (Φ) were determined using the classical formula:

$$\Phi_x = (A_s \times I_x \times n_x^2 \times \Phi_s)/(A_x \times I_s \times n_s^2) \quad (1)$$

where A is the absorbance at the excitation wavelength, I the integrated emission intensity and n the refractive index. Subscripts s and x refer to the standard and to the sample of unknown quantum yield, respectively. Coumarin 153 (Φ_s = 0.53) in ethanol was used as the standard [47]. The absorbance of the solutions was equal or below 0.06 at the excitation wavelength. The error on the quantum yield values is estimated to be about 10 %.

Emission decay curves of dilute solutions (Abs at λ_{ex}< 0.1) were recorded using the time-correlated single-photon counting method (TCSPC) on a HORIBA Fluorolog 3-2(iHR320) spectrofluorometer equipped with a nanoled-370 (λ_{ex} = 371 nm). Emitted photons were detected at 90° through a monochromator by means of a Hamamatsu R928 photomultiplier. Emission was recorded near the maximum with a bandpass of 10-15 nm. The instrumental response was recorded directly on the sample at 370 nm before each decay curve. All analyses were recorded using the Datastation v2.7 software. The decay curves were analyzed with reconvolution and global non-linear least-squares minimization method using DAS6 v6.8 software. The rate constants for radiative (k_r) and nonradiative (k_{nr}) decay were calculated as follows:

$$k_r = \Phi/\tau \text{ and } k_{nr} = (1-\Phi)/\tau \quad (2)$$

with Φ the emission quantum yield and τ the luminescence lifetime in solution.

Solid state spectra were recorded on the same Xenius SAFAS spectrofluorometer equipped with an integrating sphere and corrected using a home-made correction curve. Solid samples were deposited on a metal support. The absolute photoluminescence quantum yield values (Φ_P) were determined by a method based on the one developed by de Mello *et al* [48], as described elsewhere [41]. The error was estimated to be about 20%.

Fluorescence microscopy was performed with a Leitz Laborlux D fluorescence microscope equipped with an Andor Luca camera.

2.6 Computational details

The ORCA software was employed for all calculations (the geometry optimization, the ground-state and excited-state electronic structures, and optical spectra) with the aid of the Gabedit

visualization program [49]. Density functional theory (DFT) and time-dependent DFT (TD-DFT) calculations were performed with the PBE0 functional [50]. The ground state (S_0) and the lowest triplet state (T_1) geometries of compounds were fully optimized with the DFT method using the Perdew-Burke-Ernzerhof PBE0 functional without symmetry constraints [51]. In all calculations, the "double-ζ" quality basis set LANL2DZ with Hay and Wadt's relative effective core potential ECP (outer-core [($5s^2 5p^6$)] electrons and the ($5d^6$) valence electrons) [52, 53] was employed for the Re^+ cation. The solvent effect (DCM, ε = 9.08) was simulated using the Conductor-like Polarizable Continuum Model (CPCM) [54, 55]. The vibrational frequency calculations were performed using the optimized structural parameters of compounds, to confirm that each optimized structure represents a local minimum on the potential energy surface. On the basis of the optimized ground state geometry, the absorption properties were calculated by the TD-DFT method at the PBE0/LANL2DZ level. The emission has been calculated by DFT considering the difference of energy between the optimized triplet state and the singlet state at the same geometry. Orbital compositions have been calculated using Multifwn software [56] with the orbital composition analysis (Mulliken partition) function [57].

3 Results and discussion

3.1 Synthesis and characterization

Complex **1-Cl** was already available from our previous work [42]. The other two complexes were obtained using the same general procedure (Fig. 2). The bidentate ligand **L1** was prepared in 60% yield by condensation of aniline on 2-(pyridin-2-yl)-1,3,4-oxadiazole in the presence of catalytic *p*-TsOH in refluxing xylenes. Then this ligand was reacted with commercially available [$ReBr(CO)_5$] in refluxing methanol to obtain tricarbonylrhenium(I) complex **1-Br** in 70% yield. The reaction of ligand **L1** with freshly prepared [$ReI(CO)_5$] [43] resulted in the formation of complex **1-I**, which did not precipitate in the medium, contrary to its chloride and bromide counterparts, and was obtained in a modest yield of 33% after purification by column chromatography.

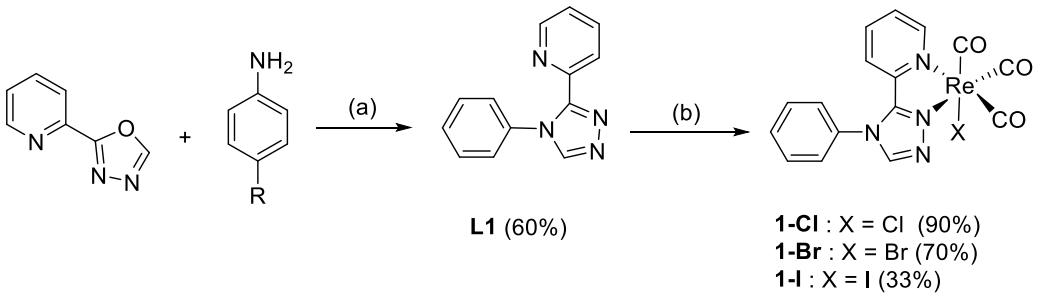

Fig. 2 Synthesis of complexes **1-Cl** (from ref. 42), **1-Br** and **1-I**. Conditions and reagents: (a) *p*-TsOH, xylenes, 140°C, 24h. (b) [$Re(CO)_5X$] (X = Cl, Br, I), MeOH, 65°C, 16 h.

The complexes were identified by ^1H and ^{13}C NMR (Fig. S2-S5†, ESI), high resolution mass spectrometry and their purity was checked by elemental microanalyses. It can be seen that the ^1H NMR signals corresponding to the pyta protons are deshielded by 0.10-0.15 ppm with respect to **1-Cl** (Fig. S6†, ESI), indicating a slight decrease of the electron density. A similar

evolution can be found in the literature for complexes built from other N^N ligands [5, 58]. The Fourier transform infrared (FTIR) spectra of the complexes in dichloromethane (DCM) solutions showed the stretching bands that are the characteristic signature of the three CO groups in a *fac*-[Re(CO)$_3$] arrangement. The average value of these bands, which reflects the electron density at the metal center [59] was very slightly increased from 1950 cm^{-1} for **1-Cl** to 1952 cm^{-1} for **1-Br** and 1953 cm^{-1} for **1-I**.

The stability of the complexes dissolved in DCM was monitored by ^{1}H NMR over five days in the dark. No significant evolution of the ^{1}H NMR spectra was detected, suggesting a good chemical stability. No variation was observed either by leaving the samples at the ambient light for 24 h. No troublesome photochemical instability was noted when performing the physico-chemical experiments described below. However, the three complexes were used with utmost care, and a thorough photochemical study, carried out under energetic irradiation conditions, will be the subject of further work.

3.2 Crystal structures

X-Ray quality crystals of the complexes **1-Br** and **1-I** were grown by slow evaporation of chloroform solutions. Selected crystallographic data are collected in the experimental section (Table 1) and in the ESI (Tables S1† and S2†, Fig. S7†). Previously published data about **1-Cl** [42] are used for the sake of comparison. As expected, the coordination sphere of the three complexes exhibits a slightly-distorted octahedral geometry, in which the rhenium atom is coordinated to three carbonyl groups in a *fac* configuration, two nitrogen atoms of the pyta ligand and one halogen atom. However, some lengths and angles of the coordination sphere are different in the three complexes. In particular, the bond between the rhenium and halogen atoms passes from 2.474(2) Å for **1-Cl** to 2.602(1) Å for **1-Br**, and then to 2.799(1) Å for **1-I**, thus increasing with the size of the halogen atom.

For the three complexes, the asymmetric unit contains two molecules that correspond to two distinct eniantiomers, in which the phenyl group is either at the left side or at the right side of the CO-Re-X axis, if the latter is considered in the same orientation (Fig. 3 and Fig. S7–S9†). The dihedral angle between the phenyl and triazole rings is a strong indicator of the molecular geometry. This angle has a value of 50.7(9)° and 84.6(8)° for the two molecules that constitute the asymmetric unit of **1-Br**, 54.3(11)° and 88.8(9)° for those of **1-I**, indicating that for both compounds one molecule is much more twisted than the other one. In sharp contrast, the two molecules of the asymmetric unit of **1-Cl** have similar dihedral angles of 68.7(13)° and 67.9(13)°.

The molecular arrangement is almost the same for **1-Br** and **1-I**. Whatever the ring considered, its center of gravity is distant by more than 4 Å from any ring of a neighboring molecule. The only exception is for the triazole rings that are quite close from each other (3.7–3.8 Å), so that the corresponding molecules form a sort of antiparallel dimer (Fig. S8†). In contrast, for **1-Cl**, the triazole rings are quite far apart (4.15 Å), while the shortest distance is found between the pyridyl rings of two neighboring molecules (3.87 Å) (Fig. S9†). In the three cases, no overlaps of the aromatic systems are detected. The halogen atoms are involved in five distinct short contacts with neighboring molecules, the mean distance of which increases from 2.77 Å for **1-Cl** to 3.04 Å for **1-Br** and 3.27 Å for **1-I**. Therefore, they strongly structure the network (Fig. 4). This is also the case for the CO groups, and for the pyridyl nitrogen atom N3 for **1-Br** and **1-I** (Fig. S8†). The shortest distance between two rhenium atoms are quite similar (6.42 for **1-Cl**, 6.44 Å for **1**-Br and 6.33 Å for **1-I**). Noticeably, in **1-Br** and **1-I**, which are

chloroform solvates, the molecules of complexes are displayed in layers separated by columns of solvent (Fig. 5).

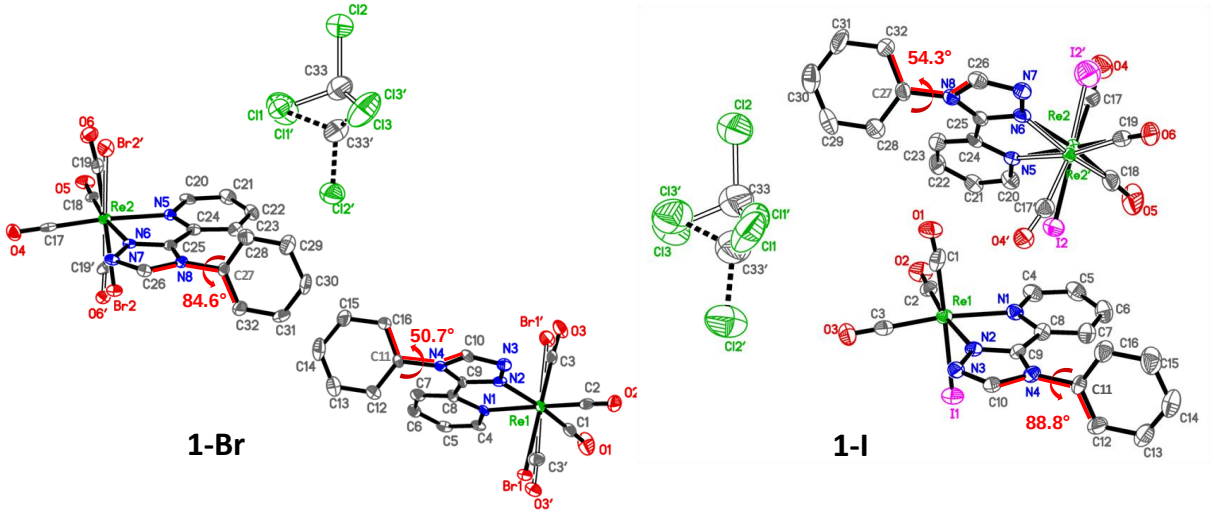

Fig. 3 Molecular view of the asymmetric unit of complexes **1-Br** and **1-I**, with phenyl-pyta dihedral angles indicated in red. Hydrogen atoms are not represented for the sake of clarity. Displacement ellipsoids are drawn at 50% probability. The labels (') correspond to the minor part of the disorder, which is in every case lower than 10%.

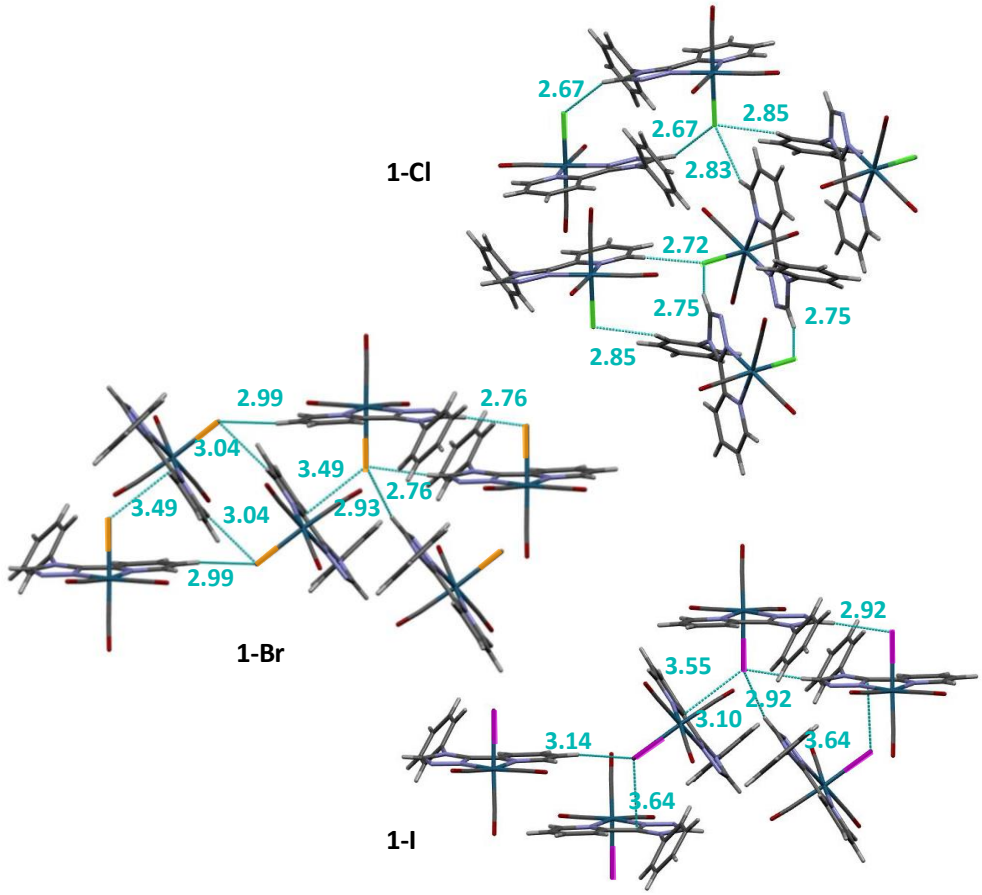

Fig. 4 Crystallographic arrangement of complexes **1-Cl** (from ref. 42), **1-Br** and **1-I** showing the short contacts (distances in Å) that involve the halogen atoms drawn in green, orange and purple, respectively.

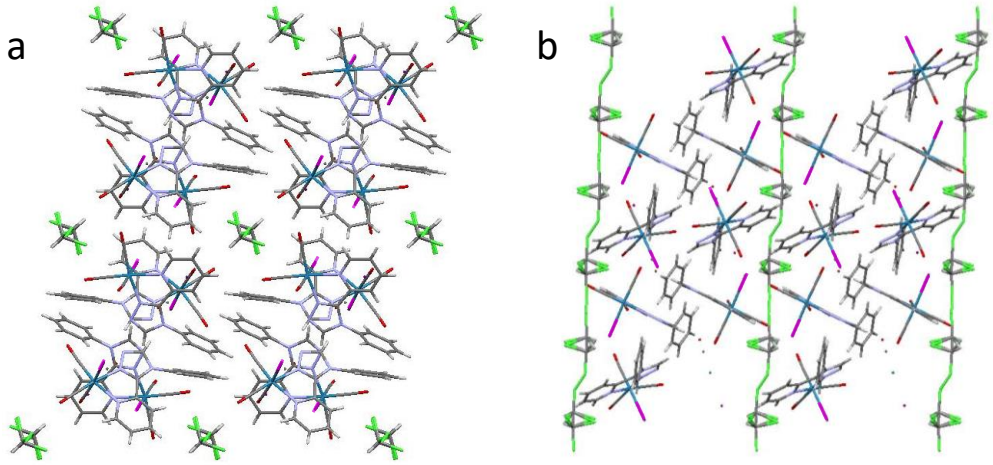

Fig. 5 Molecular packing in a crystal of complex **1-I**. a) view along axis *a*. b) view along axis *b*.

3.3 Electronic structure and transitions

The full results of computational studies based on the density functional theory (DFT) method and the time-dependent DFT (TD-DFT) method for complexes **1-Br** and **1-I** in DCM can be found in the ESI, together with the composition of the frontier molecular orbitals involved in the main electronic transitions for **1-Cl** (Tables S3† to S8†, Fig. S10† to S16†). Figure 6 shows the isodensity plots for the four frontier orbitals of the three complexes. In the electronic ground state, the molecules are characterized by a d^6 electronic configuration of the rhenium atom and low-lying π^* orbitals localized on the organic ligand. The electron density of the highest occupied molecular orbitals (HOMOs) is localized on the rhenium atom, the carbonyl ligands and the halogen atom. Remarkably, the HOMO and HOMO-1, which have almost the same orbital composition and close energy levels, exhibit pronounced differences according to the nature of the halide ligand. In fact, if considering for example the HOMO, the electron density localized on the halogen atom increases remarkably from 25.4% for **1-Cl** to 41.0% for **1-Br**, and then to 63.6% for **1-I**, and the contribution of the electron density on the rhenium atom decreases concomitantly (47.4%, 37.8% and 23.8%, respectively) (Tables S3†, S5† and S7†). The values are very close for the HOMO-1. The X/Re electron density ratio can be calculated to be 0.53, 1.08, and 2.67 for the HOMO of **1-Cl**, **1-Br** and **1-I**, respectively, and 0.63, 1.30 and 3.05 for their HOMO-1. These results are in line with those published about $[ReX(CO)_3(bpy)]$ (X= Cl, Br, I; bpy = 2,2'-bipyridine) [30, 32]. In contrast to the HOMOs, the lowest unoccupied molecular orbitals (LUMOs), which are centered on the organic ligand, hardly vary from one complex to the other. The electron density is first localized on the pyta moiety, and then its importance on the phenyl group increases with increasing the orbital number. Regarding the energy levels, that of the HOMOs increases significantly with increasing the size of the halogen atom, while the level of the LUMOs remains quite constant. Consequently, the HOMO-LUMO gap decreases in the order: 4.04 eV for **1-Cl**, 3.96 eV for **1-Br** and 3.80 eV for **1-I** (Fig. 6).

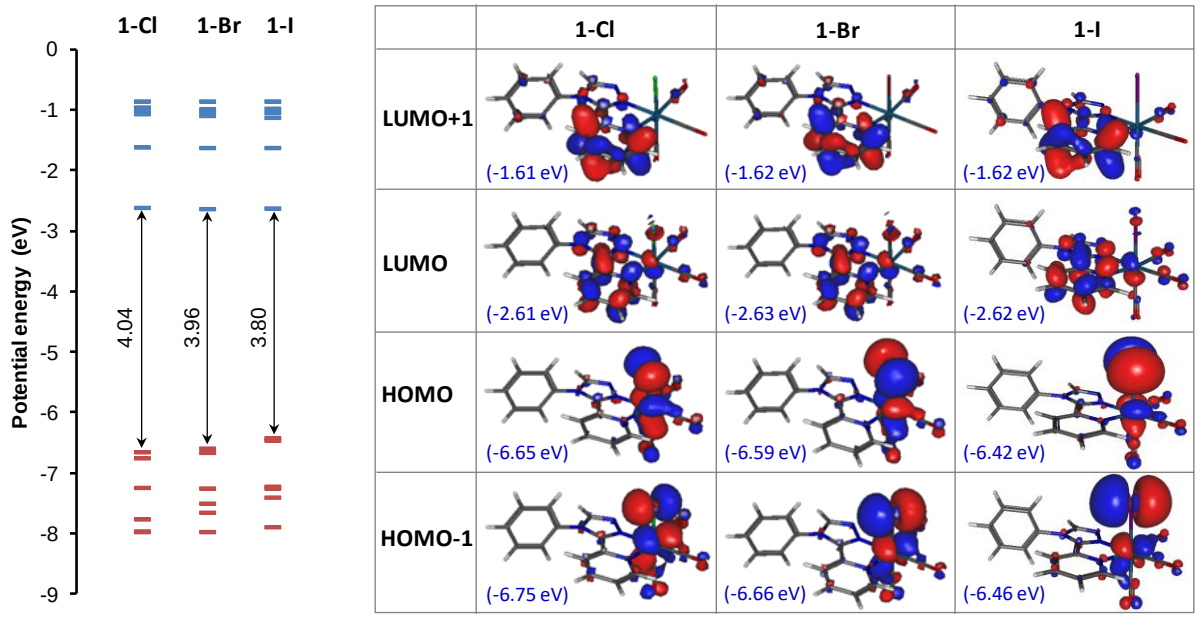

Fig. 6 Left: Comparison of the potential energy of the six first HOMOs and LUMOs, and HOMO-LUMO energy gap; Right: Isodensity plots (isovalue = 0.03) and energy levels of the first frontier molecular orbitals, for complexes **1-Cl**, **1-Br** and **1-I** in dichloromethane, according to DFT calculations at the PBE0/LANL2DZ level of theory.

For the three complexes, the lowest energy transition associated with high oscillation strength is a HOMO-1→LUMO transition with mixed metal to ligand charge transfer (MLCT) and halide to ligand charge transfer (XLCT) character. For **1-Cl**, the contribution of MLCT is preponderant, and the transition is predicted at 418.2 nm. For **1-Br** and **1-I**, this transition has strong XLCT character, and it is expected at 443.8 nm and 498.4 nm, respectively. Between 300 and 360 nm, the transitions occur from the five first HOMOs towards the LUMO and LUMO+1. They have XLCT/MLCT character for **1-Br** and **1-Cl**, and MLCT/XLCT character for **1-I**, with ligand to ligand charge transfer (LLCT) contribution especially for **1-Cl**. Finally, many high-energy transitions, which may involve high-numbered orbitals, have mixed XLCT/MLCT/LLCT and intra-ligand charge transfer (ILCT) character.

3.4 Electrochemical studies

The electrochemical behavior of complexes **1-Br** and **1-I** was studied by cyclic voltammetry (CV) and Osteryoung square wave voltammetry (OSWV) measurements in DCM at room temperature (Fig. S18† to S26†), and the results were compared with those previously published for **1-Cl** [42]. The electrochemical characteristics of **1-I** are different from those of **1-Br** and **1-Cl**. Indeed, in the OSWV anodic part, the first oxidation potential of **1-I** is at 1.26 V, around 0.2 V lower than that of the other two complexes, thus indicating a better electron donating capability of this species (Table S9†, Fig. S18† and S21†). Moreover, as shown in Fig. 7, the intensity of this process is not in a 1/1 ratio when compared to the first one-electron reduction process (around –1.30 V), contrary to what is observed for the **1-Cl** and **1-Br** complexes (Fig. 7 and S25†) and for other derivatives of this family. This first reduction process can be attributed to the reduction process of the substituted triazole ring, the value of which may be substantially decreased by complexation, as observed in related compounds [60, 61]. As

previously proposed, the value of this first reduction process seems to be characteristic of this family of complexes incorporating a 2-pyridyl-1,2,4-triazole ligand [40–42] and could be related to the bent arrangement of the pyta moiety with its connected moiety as illustrated by the X-ray structures. In CV, the careful examination of the first reduction process at different scan rates showed that the latter becomes quasi-reversible at around 1 V s^{-1} for compound **1-Cl**, 5 V s^{-1} for complex **1-Br**, and slightly more reversible at 50 V s^{-1} for **1-I**, suggesting the formation of a more stable one-electron reduction species in solution for the Cl compound with respect to the others.

Considering further the OSWV anodic part of the **1-I** compound, a second and minor oxidation process is also observed at 1.48 V. This potential value is close to that found for the first one-electron oxidation process of the **1-Br** and **1-Cl** complexes (Fig. S25†**)**, which can be mainly assigned to an irreversible Re(I)/Re(II) oxidation process [62, 63].

Importantly, for each of the three complexes, the values of both the electrochemical gap and the calculated HOMO-LUMO gap are in good agreement (Table S10†). These gaps are smaller for **1-I** than for **1-Cl** and **1-Br**. Considering that the value of the first reduction potential is nearly the same for the three compounds, this difference comes from the lower oxidation potential of the **Re-I** compound (at 1.26 V), as confirmed by the higher value of the HOMO energy level. Looking at the composition of the frontier molecular orbitals of the three complexes (see above), it was noticed that the HOMO is significantly centered on the Re atom for the **1-Br** and **1-Cl** complexes, and on the iodine atom for the **1-I** complex. Consequently, under our standard electrochemical conditions, it may be proposed that for the **1-I** complex, the first oxidation process in solution involves the iodine atom. As the strength of the Re-I bond is weaker than that of the Re-Cl and Re-Br bonds (see crystallographic data), upon oxidation of the iodine atom, some decomposition of the complex could happen and/or some iodine reactivity could take place with traces of water or by-products formed in the electrochemical medium [64]. Consequently, the current intensity of the first irreversible oxidation process of **1-I** may be weaker than that observed for its Cl and Br counterparts. To sum up, electrochemistry appears here as a useful tool to clearly evidence in solution two major changes that occur when substituting the Cl or Br atom by the I atom in the initial framework of the molecule, *i.e.* a change in the nature of the HOMO and a decrease of the HOMO-LUMO gap, as confirmed by theoretical calculations.

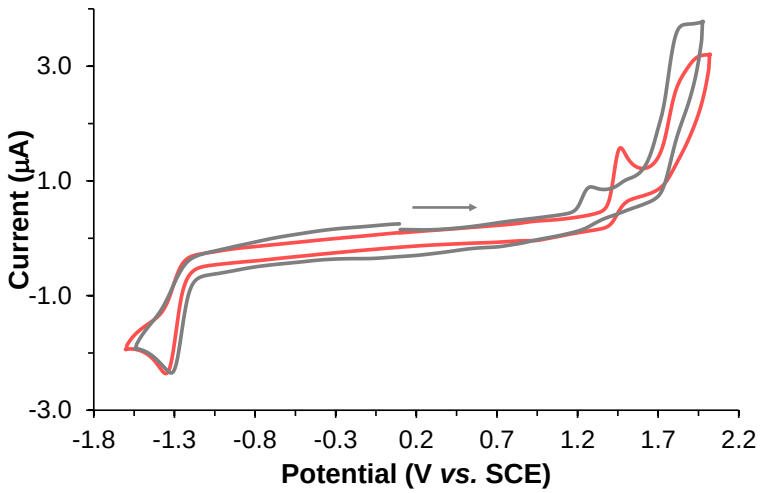

Fig. 7 Cyclic voltammograms of **1-Br** (orange line) and **1-I** (grey line) complexes in CH_2Cl_2 + 0.1 M [nBu$_4$N][BF_4], recorded with a Pt working electrode at room temperature and at a scan rate of 0.2 Vs^{-1} towards anodic potentials.

3.5 UV-visible absorption and emission properties

All spectroscopic data have been gathered in Table 2. The experimental UV-visible absorption spectra of the three complexes were recorded in DCM (Fig. 8). Two intense high-energy bands peaked below 300 nm. A shoulder was visible around 320 nm only for **1-I**. Then, a moderately intense band appeared at long wavelengths, between the near UV and the beginning of the visible range. Its maximum was markedly shifted to the red with increasing the size of the halogen atom (382 nm for **1-Cl**, 388 nm for **1-Br** and 400 nm for **1-I**). The experimental spectra were situated at higher energy (0.3–0.4 eV) than predicted by the calculation. Such a discrepancy, attributable to intramolecular motions that are not taken into account by calculations, is at the limit of what is acceptable when using DT-DFT [65]. The molar extinction coefficient was almost the same for the chloride and bromide complexes, for which the corresponding transition has a predominant MLCT character, but it was decreased by more than one third for the iodide complex, probably due to the strong XLCT character of the transition [32].

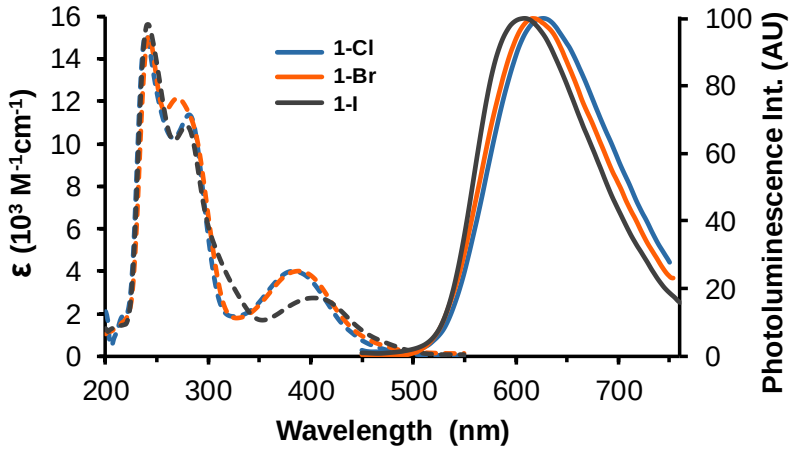

Fig. 8 UV-vis absorption spectra (dashed lines) and normalized emission spectra (solid lines) of complexes **1-Cl** (blue line), **1-Br** (orange line) and **1-I** (grey line) in air-equilibrated dichloromethane. Concentrations ~ 7×10^{-5} M for absorption, ~ 1.8×10^{-5} M to 3.4×10^{-5} M for emission. Excitation at the maximum wavelength of the low-energy absorption band.

The excitation spectra in DCM were very close to the absorption spectra. The emission spectra displayed only one unresolved band, the maximum of which was red-shifted in the order **1-I** (608 nm) < **1-Br** (616 nm) < **1-Cl** (626 nm). The emission quantum yields were below 3% in aerated solutions. After bubbling with argon, they were multiplied by 2.5, 1.8 and 1.4, for **1-I**, **1-Br** and **1-Cl**, respectively, and this effect was perfectly reversible. The luminescence decays were monoexponential. In aerated solutions, the lifetime, of the order of one hundred of nanoseconds, was almost multiplied by two when passing from **1-Cl** to **1-I** explaining why the sensitivity of the complexes towards oxygen increases in the same order. The rate of the radiative deactivation constant k_r was very slightly changed for the three complexes, while the rate of the nonradiative deactivation constant k_{nr} was markedly decreased upon going from **1-Cl** to **1-I**. This observation can be explained by the MLCT/XLCT change in character of the emitting excited state upon going from Cl to I. Most likely, the MLCT excited state of **1-Cl** and **1-Br** is mainly deactivated *via* vibrations of the bonds between Re and the organic ligand, while this deactivation pathway becomes much less important for **1-I** [32].

	Dichloromethane [a]									Solid state					
										Pristine		Ground		THF Fumed	
	λ_{abs} [nm]	ε [$M^{-1}cm^{-1}$]	$\lambda_{P\ exp}$ [nm]	$\lambda_{P\ calc}$ [nm]	Φ_P	τ [ns]	χ^2	k_r [$10^5\ s^{-1}$]	k_{nr} [$10^5\ s^{-1}$]	λ_{PL} [nm]	Φ_{PL}	λ_{PL} [nm]	Φ_{PL}	λ_{PL} [nm]	Φ_{PL}
1-Cl [b]	240	15100	626 [c]	606	0.020	74.7 [c]	1.29	2.67	131.19	550	0.42	560	0.13	550	0.23
	282	11600													
	382	4000													
1-Br	240	15100	616 [d]	601	0.029	115.1 [d]	1.19	2.52	84.36	558	0.19	576	0.11	556	0.21
	270	11900													
	388	3900													
1-I	238	15600	608 [d]	604	0.022	134.3 [d]	1.50	1.64	72.82	556 [e]	0.11 [e]	578 [e]	0.05 [e]	558 [e]	0.18 [e]
	278	10600								549 [f]	0.13 [f]	569 [f]	0.05 [f]	553 [f]	0.09 [f]
	400	2500													

[a] Air-equilibrated solutions. Concentrations: ~ 7×10^{-5} M for absorption, ~ 1.8×10^{-5} M to 3.4×10^{-5} M for emission. [b] From ref. 42. [c] λ_{ex} = 371 nm. [d] Excitation near the maximum wavelength of the low-energy band. [e] Complex obtained from CH_2Cl_2. [f] Complex crystallized from $CHCl_3$.

Table 2 Spectroscopic data of the three complexes in dichloromethane solution and in the solid state. Maximum wavelengths of absorption (λ_{abs}), experimental and calculated phosphorescence emission ($\lambda_{P\ exp}$ and $\lambda_{P\ calc}$), excitation (λ_{ex}) and photoluminescence (λ_{PL}); molar extinction coefficient (ε), phosphorescence and photoluminescence quantum yields (Φ_P and Φ_{PL}), lifetime (τ) and chi squared value (χ^2), radiative (k_r) and non-radiative (k_{nr}) deactivation constants.

The rather long lifetimes indicate that the emission detected is mainly phosphorescence, as commonly reported for this type of complexes. Moreover, the maximum wavelengths are close to those calculated for emission arising from the first excited triplet state T_1 (Table 2). It must be emphasized that our DFT calculations consider that the lowest energy transition is a LUMO→HOMO, but a LUMO→HOMO-1 transition is also possible. The lowest energy absorption is due to a HOMO-1→LUMO transition, and it seems that for our three complexes the triplet hole orbital compares better with the HOMO-1 than with the HOMO (Fig. S17†). However, since the energy levels of the HOMO and HOMO-1 are very close, the predicted emission wavelength changes little if considering any of these two ground state orbitals. A TD-DFT study of the whole deexcitation process from absorption to emission through vibrational relaxation and spin-orbit coupling would be necessary to clear up this ambiguity. The comparison with the literature data [28–30, 32] confirms our results and sheds some new light on them. According to Gourlaouen *et al*. [30], only the first triplet state T_1 is responsible for the phosphorescence emission of both the chloride and bromide [$ReX(CO)_3(bpy)$] complexes in solution. In contrast, for the iodide complex, the second triplet state T_2, very close to T_1, also contributes to the phosphorescence emission. Other significant variations have been reported in the photophysics of this type of complexes according to the nature of the halide ligand. We do not have the means to carry out such thorough photophysical and theoretical studies, which could show spectacular differences between our three complexes. What we see is that, despite the small variations commented above, there are no drastic changes of the spectroscopic properties in solution. A simple explanation is that this type of complexes undergoes more or less strongly the heavy-atom effect due to rhenium, possibly combined with the heavy-atom effect due to the halogen atom. For instance, the low-lying excited states of **1-Cl** have a pronounced metal character, and so the heavy atom effect of the rhenium atom totally governs the spectroscopic properties. In **1-Br**, the metal character is weaker than in **1-Cl**, but it is counterbalanced by the heavy atom effect due to the bromine atom. In **1-I**, the heavy-atom effect due to the iodine atom becomes preponderant. The result of both effects makes that, from a practical point of view, all three complexes in solution emit weak orange-red phosphorescence.

Let us now turn our attention towards the solid-state spectroscopic properties. The excitation of the three yellow microcrystalline powders by a hand-held UV lamp (365 nm) generated strong yellow light. The solid-state luminescence enhancement (SLE) effect [66] is therefore clear for the three complexes. The excitation spectra revealed the presence of two bands in the UV (374 nm) and in the visible range (472 nm), and it was checked that the powders can indeed be excited at both wavelengths. The emission spectra showed one unresolved band (Fig. 9a) peaking at 558 nm for **1-Br**, *i.e.* slightly shifted to the red with respect to **1-Cl** (550 nm). The maximum emission of **1-I** varies between these values depending on whether the samples were prepared in DCM or chloroform, which probably has an influence on the crystal packing mode. Noticeably, the high photoluminescence quantum yield (PLQY) of **1-Cl** (0.42) was reduced by more than half for **1-Br** (0.19), and reduced again when passing from **1-Br** to **1-I** (0.11–0.13). This evolution could be related to the geometry of the complexes in the crystals. In fact, for **1-Cl**, the two molecules that constitute the asymmetric crystal unit exhibit a phenyl-pyta dihedral angle close to 68°, intermediate between the calculated angle of the optimized ground state (~90°) and first triplet excited state (~50°) (Fig. S16†). A motion of moderate magnitude, probably allowed by the crystalline constraints, may thus occur so that the molecules easily reach the excited state. In contrast, one molecule that is part of the asymmetric unit of **1-Br** and **1-I** has a dihedral angle close to 50°, far from the optimal ground state geometry. It can be thought that the probability for this molecule to be excited is lower than for the molecules of **1-Cl**. Conversely, the second molecule of **1-Br** and **1-I** is blocked by the packing forces in a geometry with a dihedral angle above 84°. Excitation should be easy,

but reaching the first triplet excited state requires a large motion, possibly not allowed in the crystal. Moreover, the difference of emission efficiency between **1-Br** and **1-I** may be attributed to the molecular interactions that involve the halogen atom, and could play a major role due to the pronounced XLCT character of the T_1 state for **1-I**.

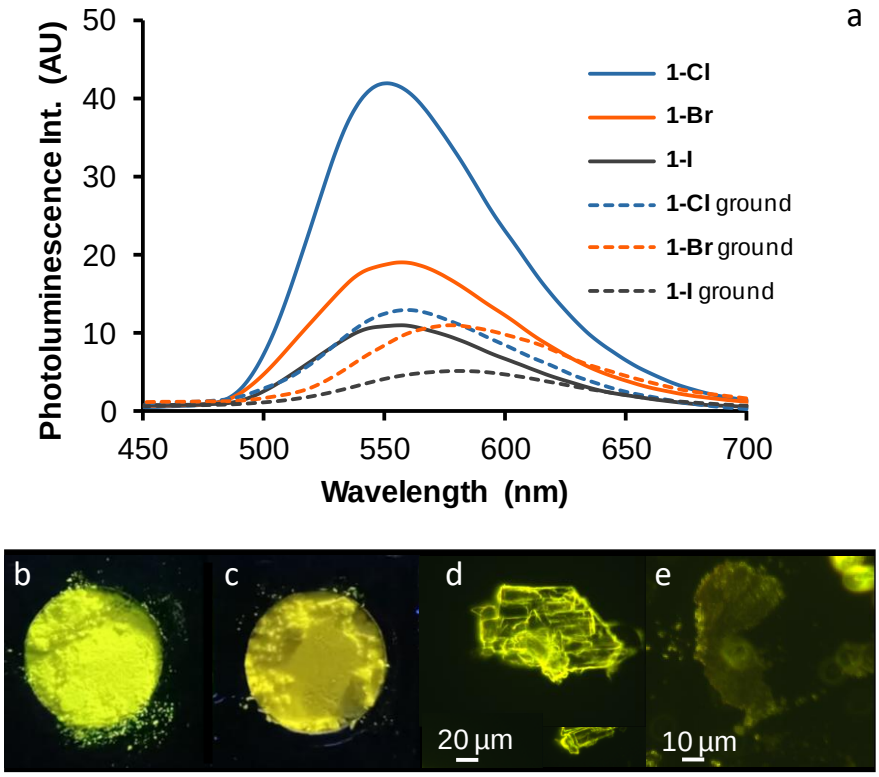

Fig. 9 a) Emission spectra of the three complexes **1-Cl** (blue line, λ_{ex} = 385 nm), **1-Br** (orange line, λ_{ex} = 388 nm), and **1-I** prepared in CH_2Cl_2 (grey line, λ_{ex} = 398 nm) as microcrystalline pristine powders (solid lines), and after grinding (dashed lines), with intensity proportional to the PLQY. b) Image of pristine powder and (c) ground powder of **1-Br** illuminated at 365 nm by a hand-held UV lamp. d) Microcrystals of **1-I** (obtained from a CH_2Cl_2 solution) under the fluorescence microscope and (e) the same sample after crushing with a spatula (λ_{ex} ~ 450−490 nm, λ_{em} > 500 nm).

It was shown previously for other complexes integrating a 1,2,4-pyta ligand that the solid-state emission spectra shift to long wavelengths upon mechanical stimuli, and the initial properties are partially restored when the sample is fumed with solvent vapors. This mechanoresponsive luminescence (MRL) effect [67] has been attributed to a reversible switch from crystalline to amorphous phases [10]. It was found here that the emission of the pristine microcrystalline powder of complexes **1-Br** and **1-I** passes from greenish yellow to orange yellow upon grinding with a mortar and a pestle (Table 2, Fig. 9a-c), or after crushing with a spatula (Fig. 9d,e). The wavelength shift, which reaches 18 nm and 22 nm for **1-Br** and **1-I**, respectively, is twice as large as that previously reported for **1-Cl** [40]. It is fully reversible when exposing the samples to tetrahydrofuran vapors. Concomitantly, a decrease of emission intensity is observed upon grinding, leading to the almost complete extinction of photoluminescence in the case of **1-I**, and subsequent PL revival is induced by THF fuming. Noticeably, the emission intensity of the fumed sample is significantly higher than that of the

pristine sample for **1-I**. One explanation may be that fuming leads to a crystal structure slightly different from that of the original solvate (Table 2, Fig. S27†). By comparison, the intensity of the fumed sample of **1-Cl** is twice less than that of the pristine sample, as frequently observed and attributed to uncompleted recovery of crystallinity.

The more pronounced MRL behavior of **1-Br** and **1-I** could be explained by their loose crystal packing mode due to the incorporation of solvent molecules (Fig. 4), while the molecules of **1-Cl** are tightly packed and thus lead to incomplete amorphization upon mechanical stimulation [68, 69]. Additional information is given by the examination of the ATR-FTIR spectra (Fig. 10). It can be noticed that the IR stretching bands corresponding to the CO ligands have a very similar shape for the three complexes in the amorphous state. The spectrum of crystalline **1-Cl** is also very close to the former ones. This is not the case for **1-Br** and **1-I**, whose ATR-FTIR spectra significantly broaden and increase in intensity when passing from

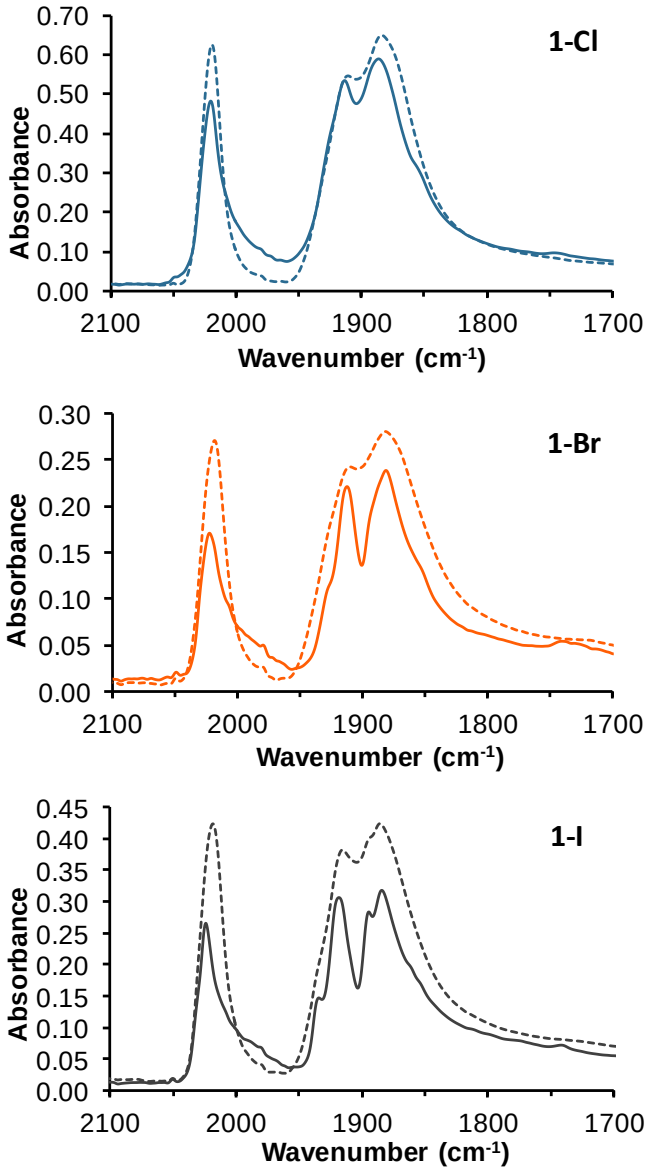

Fig. 10 ATR FTIR spectra of pristine (solid line) and ground (dashed line) powders of complexes **1-Cl**, **1-Br** and **1-I** (from top to bottom) in the region of the CO stretching bands.

pristine to ground samples. This phenomenon is possibly due to the different isomers in the crystal of **1-Br** and **1-I**, and to the fact that the molecular geometries in the crystal are quite far from those in the amorphous state, where intermolecular constraints are much weaker. In any case, this observation suggests an increased variation of the vibrational modes upon amorphization when increasing the halogen size. Possibly, this phenomenon is linked to the opening of vibrational non-radiative pathways, which may play an important role in the decrease of phosphorescence intensity [10].

Finally, the observation of the microcrystals of **1-Br** and **1-I** under the fluorescence microscope revealed that the surface was dark while a strong yellow light was emitted by the edges (Fig. 9d and S28†). This effect seems to be clearer than for microcrystals of **1-Cl** [42] possibly because of the good quality of microcrystals of **1-Br** and **1-I**. A possibility is that it arises from self-waveguided edge-emission [70, 71], a hypothesis to verify with more specialized equipment.

4 Conclusions

This systematic study shows the importance of the nature of halogen atom in tricarbonylrhenium complexes of type *fac*-[ReX(CO)$_3$(phenyl-pyta)] (X = Cl, Br, I). The evolution of the electronic properties is due to the fact that the first transitions gradually change from an MLCT character to an XLCT character, as the size of the halogen increases. For the complexes in solution, this progression is hardly visible on the spectroscopic properties, but it clearly impacts the electrochemical properties, in particular for the iodide complex. In the solid state, the photoluminescence properties, which depend on both the electronic system and the molecular arrangement, vary dramatically with the size of the halogen atom.

This study allows the various complexes to be selected in view of a given applications. On the one hand, if looking for a good solid-state emitter, *e.g.* to constitute the core of luminescent nanoparticles for bio-imaging [72], the **1-Cl** chloride complex must be preferred. This will also be the case if looking for an SLE-active luminophore, widely used for the monitoring of aggregation processes in biology [73]. For instance, we will show in a forthcoming work that a derivative of **1-Cl** functionalized by a small recognition unit allows fine detection of a bio-macromolecule. On the other hand, if MRL properties are sought, the bromide and iodide complexes **1-Br** and **1-I** should rather be considered. The color change observed upon mechanical stimuli is weaker than that of complexes bearing an aromatic group on the phenyl ring, for which a different photophysical process is involved [10]. However, the decrease of emission intensity that leads to a virtual extinction of luminescence for **1-I** may be valuable for applications. The **1-Br** bromide complex offers a good compromise between ease of synthesis, solid-state emission efficiency and MRL properties. Unexpectedly, the iodide complex **1-I** is quite chemically and photochemically stable. These two compounds, or some of their derivatives, could find applications as luminescent “smart” materials.

From a general point of view, our pyta-based complexes have proven to be excellent tools for this demonstration. Results on the properties of complexes in solution can apply to conventional types of Re(I) complexes that usually do not display special emission behavior in the solid state. Above all, our full results should be useful for optimizing the design of new photoluminescent tricarbonyl Re(I) complexes, which are still quite rare in the fields of SLE and MRL-active materials.

Conflicts of interest

There are no conflicts to declare.

Acknowledgements

We thank Dr. Alix Sournia-Saquet and Mr. Alain Moreau (LCC) for the electrochemical measurements, and the members of the LCPQ laboratory for their kind guidance and help in theoretical calculations.

References

[1] Lee, L. C.-C., Leung, K.-K., & Lo, K. K.-W. (2017). Recent development of luminescent rhenium(I) tricarbonyl polypyridine complexes as cellular imaging reagents, anticancer drugs, and antibacterial agents. *Dalton Transactions*, 46, 16357–16380. DOI: 10.1039/c7dt03465b

[2] Lo, K. K.-W. (2015). Luminescent rhenium(I) and iridium(III) polypyridine complexes as biological probes, imaging reagents, and photocytotoxic agents. *Accounts of Chemical Research*, 48, 2985–2995. DOI: 10.1021/acs.accounts.5b00211

[3] Zhao, G.-W., Zhao, J.-H., Hu, Y.-X., Zhang, D.-Y., & Li, X. (2016). Recent advances of neutral rhenium(I) tricarbonyl complexes for application in organic light-emitting diodes. *Synthetic Metals*, 212, 131–141. DOI: 10.1016/j.synthmet.2015.12.014

[4] Choroba, K., Maroń, A., Świtlicka, A., Szłapa-Kula, A., Siwy, M., Grzelak, J., Maćkowski, S., Pedzinski, T., Schab-Balcerzak, E., & Machura, B. (2021). Carbazole effect on ground- and excited-state properties of rhenium(I) carbonyl complexes with extended terpy-like ligands*Dalton Transactions*, 50, 3943–3958. DOI: 10.1039/d0dt04340k

[5] Komreddy, V., Ensz, K., Nguyen, H., & Rillema, D. P. (2020). Synthesis and characterization of rhenium(I) 4,4′-dicarboxy-2,2′-bipyridine tricarbonyl complexes for solar energy conversion. *Inorganica Chimica Acta*, 511, 119815. DOI: 10.1016/j.ica.2020.119815

[6] Ji, X., Zhang, P., Wei, W., Zhang, H., & Xia, B. (2018). Theoretical investigation on the electronic structures and spectroscopic properties as well as the features as dyes in dyesensitized solar cells of quinonoid containing Re(I) complexes. *Journal of Organometallic Chemistry*, 862, 40. DOI: 10.1016/j.jorganchem.2018.02.034

[7] Kameta, N., Aoyagi, M., & Asakawa, M. (2017). Enhancement of the photocatalytic activity of rhenium(I) complexes by encapsulation in light-harvesting soft nanotubes. *Chemical Communications*, 53, 10116. DOI: 10.1039/c7cc05337a

[8] Petyuk, M. Y., Berezin, A. S., Gushchin, A. L., Bagryanskaya, I. Yu, Baranov, A. Yu., & Artem'ev, A. V. (2021). Luminescent Re(I) scorpionates supported by tris(2-pyridyl)phosphine and its derivatives. *Inorganica Chimica Acta*, 516, 120136. DOI: 10.1016/j.ica.2020.120136

[9] Jin, G.-X., Wang, T., Sun, Y., Li, Y.-L., & Ma, J.-P. (2020). Photochromic rhenium-based molecular rectangles: Syntheses, structures, photophysical properties, and electrochemistry. *Inorganic Chem*istry, 59, 15019-15027. DOI: 10.1021/acs.inorgchem.0c01845

[10] Calupitan, J. P., Poirot, A., Wang, J., Delavaux-Nicot, B., Wolff, M., Jaworska, M., Métivier, R., Benoist, E., Allain, C., & Fery-Forgues, S. (2021). Mechanical modulation of the solid-state luminescence of tricarbonyl rhenium(I) complexes through the interplay between two triplet excited states. *Chemistry: A European Journal*, 27, 4191−4196. DOI: 10.1002/chem.202005245

[11] Piletska, K. O., Domasevitch, K. V., Gusev, A. N., Shul'gin, V. F., & Shtemenko, A. V. (2015). *fac*-Tricarbonyl rhenium(I) complexes of triazole-based ligands: Synthesis, X-ray structure and luminescent properties. *Polyhedron* 102, 699–704. DOI: 10.1016/j.poly.2015.10.030

[12] Bertrand, H. C., Clède, S., Guillot, R., Lambert, F., & Policar, C. (2014). Luminescence modulations of rhenium tricarbonyl complexes induced by structural variations. *Inorganic Chemistry*, 53, 6204−6223. DOI: 10.1021/ic5007007

[13] Gómez-Iglesias, P., Guyon, F., Khatyr, A., Ulrich, G., Knorr, M., Martín-Alvarez, J. M., Miguel, D., & Villafañe, F. (2015). Luminescent rhenium(I) tricarbonyl complexes

with pyrazolylamidino ligands: photophysical, electrochemical, and computational studies. *Dalton Transactions*, 44, 17516–17528. DOI: 10.1039/c5dt02793d

[14] Pino-Cuevas, A., Carballo, R., Muñoz, L., & Vázquez-López, E. M. (2015). Rhenium complexes of ligands based on stilbene – Synthesis, characterization, reactivity, and conformational analysis. *European Journal of Inorganic Chemistry*, 4402–4411. DOI:10.1002/ejic.201500500

[15] Wright, P. J., Affleck, M. G., Muzzioli, Skelton, S. B. W., Raiteri, P., Silvester, D. S., Stagni, S., & Massi, M. (2013). Ligand-induced structural, photophysical, and electrochemical variations in tricarbonyl rhenium(I) tetrazolato complexes. *Organometallics*, 32, 3728−3737. DOI: 10.1021/om400356n

[16] Kaim, W., Kramer H. E. A., V. Conny, & Rieker, J. (1989). Synthesis, electrochemistry and emission spectroscopy in fluid solution of four isomeric (α-diimine) $Re(CO)_3Hal$ complexes. *Journal of Organometallic Chemistry*, 367, 107−115. DOI: 10.1016/0022-328X(89)87212-2

[17] Saldías, M., Guzmán, N., Palominos, F., Sandoval-Altamirano, C., Günther, G., Pizarro, N., & Vega, A. (2019). Electronic and photophysical properties of $Re^{I}(CO)_3Br$ complexes

modulated by pyrazolyl−pyridazine ligands. *ACS Omega*, 4, 4679−4690. DOI: 10.1021/acsomega.8b03306

[18] Sun, S.-S., & Lees, A. J. (2000). Self-assembly triangular and square rhenium(I) tricarbonyl complexes: A comprehensive study of their preparation, electrochemistry, photophysics, photochemistry, and host−guest properties. *Journal of the American Chemical Society*, 122, 8956–8967. DOI: 10.1021/ja001677p

[19] Casson, L. A., Muzzioli, S., Raiteri, P., Skelton, B. W., Stagni, S., Massi, S., & Brown, D. H. (2011). N-Heterocyclic carbenes as π*-acceptors in luminescent Re(I) triscarbonyl complexes. *Dalton Transactions*, 40, 11960–11967. DOI: 10.1039/C1DT11233C

[20] Valdés, E., Cepeda-Plaza, M., Günther, G., Vega, A., Palacios, R., Gómez M. L., & Pizarro, N. (2020). An amine linker group modulates luminescent properties in a Rhenium(I) tricarbonyl complex. How can it be applied for ratiometric oxygen sensing? *Dyes and Pigm*ents, 172, 107787. DOI : 10.1016/j.dyepig.2019.107787

[21] Carreño, A., Solís-Céspedes, E., Zúñiga, C., Nevermann, J., Rivera-Zaldívar, M. M., Gacitúa, M., Ramírez-Osorio, A., Páez-Hernández, D., Arratia-Pérez, R., & Fuentes, J. A. (2019). Cyclic voltammetry, relativistic DFT calculations and biological test of cytotoxicity in walled-cell models of two classical rhenium (I) tricarbonyl complexes with 5-amine-1,10-phenanthroline. *Chemical Physics Letters*, 715, 231–238. DOI: 10.1016/j.cplett.2018.11.043

[22] Carreño, A., Páez-Hernández, D., Zúñiga, C., Ramírez-Osorio, A., Pizarro, N., Vega, A., Solis-Céspedes, E., Rivera-Zaldívar, M. M., Silva, A., & Fuentes, J. A. (2021). Exploring rhenium (I) complexes as potential fluorophores for walled-cells (yeasts and bacteria): Photophysics, biocompatibility, and confocal microscopy. *Dyes and Pigments*, 184, 108876. DOI: 10.1016/j.dyepig.2020.108876

[23] Ranasinghe, K., Handunnetti, H., Perera, I. C., & Perera, T. (2016). Synthesis and characterization of novel rhenium(I) complexes towards potential biological imaging applications. *Chemistry Central Journal*, 10:71. DOI: 10.1186/s13065-016-0218-4

[24] Chakraborty, I., Carrington, S. J., & Mascharak, P. K. (2014). Design strategies to improve the sensitivity of photoactive metal carbonyl complexes (photoCORMs) to visible light and their potential as CO-donors to biological targets. *Accounts of Chemical Research*, 47, 2603–2611. DOI: 10.1021/ar500172f

[25] Chakraborty, I., Carrington, S. J., & Mascharak, P. K. (2014) Photodelivery of CO by Designed PhotoCORMs: Correlation between absorption in the visible region and metal–CO bond labilization in carbonyl complexes. *ChemMedChem*, 9, 1266–1274. DOI: 10.1002/cmdc.201402007

[26] Gauthier, E. S., Abella, L., Hellou, N., Darquié, B., Caytan, E., Roisnel, T., Vanthuyne, N., Favereau, L., Srebro-Hooper, M., Williams, J. A. G., Autschbach, J., & Crassous, J. (2020). Long-lived circularly polarized phosphorescence in helicene-NHC rhenium(I) complexes: The influence of helicene, halogen, and stereochemistry on emission properties. *Angewandte Chemie International Edition*, 59, 8394–8400. DOI: 10.1002/anie.202002387

[27] El Nahhas, A., Cannizzo, A., van Mourik, F., Blanco-Rodríguez, A. M., Záliš, S., Vlček, A., & Chergui, M. (2010). Ultrafast excited-state dynamics of $[Re(L)(CO)_3(bpy)]^n$ complexes: Involvement of the solvent. *Journal of Physical Chemistry A*, 114, 6361–6369. DOI: 10.1021/jp101999m

[28] Cannizzo, A., Blanco-Rodríguez, A. M., El Nahhas, A., Šebera, J., Záliš, S., Vlček, A., & Chergui, M. (2008). Femtosecond fluorescence and intersystem crossing in rhenium(I) carbonyl-bipyridine complexes. *Journal of the American Chemical Society*, 130, 8967–8974. DOI: 10.1021/ja710763w

[29] Harabuchi,Y., Eng, J., Gindensperger, E., Taketsugu, T., Maeda, S., & Daniel, C. (2016). Exploring the mechanism of ultrafast intersystem crossing in rhenium(I) carbonyl bipyridine halide complexes: Key vibrational

modes and spin−vibronic quantum dynamics. *Journal of Chemical Theory and Computation*, 12, 2335−2345. DOI: 10.1021/acs.jctc.6b00080

[30] Gourlaouen, C., Eng, J., Otsuka, M., Gindensperger, E., & Daniel, C. (2015). Quantum chemical interpretation of ultrafast luminescence decay and intersystem crossings in rhenium(I) carbonyl bipyridine complexes. *Journal of Chemical Theory and Computation*, 11, 99−110. DOI: 10.1021/ct500846n

[31] Heydová, R., Gindensperger, E., Romano, R., Sýkora, J., Vlček, A., Jr., Záliš, S. & Daniel, C. Spin−orbit treatment of UV−vis absorption spectra and photophysics of rhenium (I) carbonyl-bipyridine complexes: MS-CASPT2 and TD-DFT analysis. (2012). *Journal of Physical Chemistry A*, 116, 11319−11329. DOI: 10.1021/jp305461z

[32] Rossenaar, B.D., Stufkens, D.J., & Vlček, Jr., A. (1996). Halide-dependent change of the lowest-excited-state character from MLCT to XLCT for the complexes $Re(X)(CO)_3(\alpha\text{-diimine})$ (X = Cl, Br, I; α-diimine = bpy, iPr-PyCa, iPr-DAB) studied by resonance Raman, time-resolved absorption, and emission spectroscopy. *Inorganic Chemistry*, 35, 2902−2909. DOI: 10.1021/ic9509802

[33] Wei, Q., Dai, Y., Chen, C., Shi, L., Si, Z., Wan, Y., Zuo, Q., Han, D., & Duan, Q. (2018). Aggregation-induced phosphorescent emission enhancement (AIPEE) Re(I) complexes: Synthesize, photophysical and theoretical simulations. *Journal of Molecular Structure*, 1171, 786–792. DOI: 10.1016/j.molstruc.2018.06.058

[34] Hu, Y.-X., Zhao, G.-W., Dong, Y., Lü, Y.-L., Li, X., & Zhang, D.-Y. (2017). New rhenium(I) complex with thiadiazole-annelated 1,10-phenanthroline for highly efficient phosphorescent OLEDs. *Dyes and Pigments*, *137*, 569–575. DOI: 10.1016/j.dyepig.2016.10.048

[35] Wang, Z., Wang, Y., Xu, Y., Li, J., Ke, X., Jia, C., Si, Z., Wan, Y., & Duan, Q. (2020). AIPE Re(I) complexes with multifunctionalized 2,2'-bipyridine as ligands: Synthesis and optical properties. *Optical Materials*, 105, 109876. DOI: 10.1016/j.optmat.2020.109876

[36] Ghodbane, A., Saffon, N., Blanc, S., & Fery-Forgues, S. (2015). Influence of the halogen atom on the solid state fluorescence properties of 2-phenyl-benzoxazole derivatives. *Dyes and Pigments*, 113, 219–226. DOI:10.1016/J.DYEPIG.2014.08.011

[37] Sonoda, Y., Goto, M., Matsumoto, Y., Shimoi, Y., Sasaki, F., & Furube, A. (2016). Halogenated (F, Cl, Br, or I) diphenylhexatrienes: Crystal structures, fluorescence spectroscopic properties, and quantum chemical calculations. *Crystal Growth & Design*, 16, 4060–4071. DOI: 10.1021/acs.cgd.6b00590

[38] Li, H., Shu, H. Y., Liu, Y., Wu, X. F., Tian, H. K., Tong, H., & Wang, L. X. (2019). Aggregation-induced emission of highly planar enaminone derivatives: Unexpected fluorescence enhancement by bromine substitution. *Advanced Optical Materials*, 7, 1801719. DOI: 10.1002/adom.201801719

[39] Gayathri, P., Karthikeyan, S., Moon, D., & Anthony, S. P. (2019). Halogen atom and position dependent strong enhancement of solid-state fluorescence and stimuli responsive reversible fluorescence switching. *ChemistrySelect*, 4, 3884–3890. DOI: 10.1002/slct.201900145

[40] Wang, J., Delavaux-Nicot, B., Wolff, M., Mallet-Ladeira, S., Métivier, R., Benoist, E., & Fery-Forgues, S. (2018). The unsuspected influence of the pyridyl-triazole ligand isomerism upon the electronic properties of tricarbonyl rhenium complexes: an experimental and theoretical insight. *Dalton Transactions*, 47, 8087–8099. DOI: 10.1039/C8DT01120F

[41] Wang, J., Poirot, A., Delavaux-Nicot, B., Wolff, M., Mallet-Ladeira, S., Calupitan, J. P., Allain, C., Benoist E., & Fery-Forgues, S. (2019). Optimization of aggregation-induced phosphorescence enhancement in mononuclear tricarbonyl rhenium(I) complexes: the influence of steric hindrance and isomerism. *Dalton Transactions*, 48, 15906–15916. DOI: 10.1039/C9DT02786F

[42] Poirot, A., Vanucci-Bacqué, C., Delavaux-Nicot, B., Leygue, N., Saffon-Merceron, N., Alary, F., Bedos-Belval, F., Benoist, E., & Fery-Forgues, S. (2021) Phenyl-1,2,4-pyta-tricarbonylrhenium(I) complexes: Combining a simplified structure and steric hindrance to modulate the photoluminescence properties. *Dalton Transactions*. 50, 13686–13698. DOI: 10.1039/D1DT02161C

[43] Darst, K. P. & Lukehart, C. M. (1979). Reactions of coordinated molecules: XX. An unexpected route to the preparation of hydroxycarbenoid and formylrhenium(I) halide complexes. *Journal of Organometallic Chemistry*, 171, 65–71. DOI: 10.1016/S0022-328X(00)88064-X

[44] SADABS, Program for data correction, Bruker-AXS.

[45] Sheldrick, G. M. (2015). SHELXT-Integrated space-group and crystal-structure determination. *Acta Crystallographica A*, 71, 3–8. DOI: 10.1107/S2053273314026370

[46] Sheldrick, G. M. (2015). Crystal structure refinement with SHELXL. *Acta Crystallographica C*, 71, 3–8. DOI: 10.1107/S2053229614024218

[47] Suzuki, K., Kobayashi, A., Kaneko, S., Takehira, K., Yoshihara, T., Ishida, H., Shiina, Y., Oishi S., & Tobita, S. (2009). Reevaluation of absolute luminescence quantum yields of standard solutions using a spectrometer with an integrating sphere and a back-thinned CCD detector. *Physical Chemistry Chemical Physics*, 11, 9850–9860. DOI: 10.1039/B912178A

[48] De Mello, J. C., Wittmann, H. F., & Friend, R. H. (1997). An improved experimental determination of external photoluminescence quantum efficiency. *Advanced Materials*, 9, 230–232. DOI: 10.1002/adma.19970090308

[49] Allouche, A.-R. (2011). Gabedit—A graphical user interface for computational chemistry softwares. *Journal of Computational Chemistry*, 32, 174–182. DOI: 10.1002/jcc.21600

[50] Adamo, C. & Barone, V. (1999). Toward reliable density functional methods without adjustable parameters: The PBE0 model. *The Journal of Chemical Physics*, 110, 6158–6170. DOI: 10.1063/1.478522

[51] Perdew, J. P., Burke, K., & Ernzerhof, M. (1996). Generalized gradient approximation made simple. *Physical Review Letters*, 77, 3865–3868. DOI: 10.1103/PhysRevLett.77.3865

[52] Hay, P. J. & Wadt, W. R. (1985). *Ab initio* effective core potentials for molecular calculations. Potentials for the transition metal atoms Sc to Hg. *The Journal of Chemical Physics*, 82, 270–283. DOI:10.1063/1.448799

[53] Hay, P. J. & Wadt, W. R. (1985). *Ab initio* effective core potentials for molecular calculations. Potentials for K to Au including the outermost core orbitals. *The Journal of Chemical Physics*, 82, 299–310. DOI: 10.1063/1.448975

[54] Mennucci, B. & Tomasi, J. (1997). Continuum solvation models: A new approach to the problem of solute's charge distribution and cavity boundaries. *The Journal of Chemical Physics*, 106, 5151–2158. DOI: 10.1063/1.473558

[55] Cossi, M., Barone, V., Mennucci, B., & Tomasi, J. (1998). *Ab initio* study of ionic solutions by a polarizable continuum dielectric model. *Chemical Physics Letters*, 286, 253–260. DOI: 10.1016/S0009-2614(98)00106-7

[56] Lu, T. & Chen, F. (2012). Multiwfn: A multifunctional wavefunction analyzer. *Journal of Computational Chem*istry, 33, 580–592. DOI: 10.1002/jcc.22885

[57] Lu, T. & Chen, F. (2011) Calculation of molecular orbital composition. *Acta Chimica Sinica*, 69, 2393–2406. http://sioc-journal.cn/Jwk_hxxb/CN/abstract/abstract340458.shtml [58] Staal, L. H., Oskam, A., & Vrieze, K. (1979). The syntheses and coordination properties of $M(CO)_3X(DAB)$ (M = Mn, Re; X = Cl, Br, I; DAB = 1,4-diazabutadiene). *Journal of Organometallic Chemistry*, 170, 235–245. DOI: 10.1016/S0022-328X(00)81088-8

[59] Suntrup, L., Klenk, S., Klein, J., Sobottka, S., & Sarkar, B. (2017). Gauging donor/acceptor properties and redox stability of chelating click-derived triazoles and triazolylidenes: A case study with rhenium(I) complexes. *Inorganic Chemistry*, 56, 5771−5783. DOI: 10.1021/acs.inorgchem.7b00393

[60] Lo, W. K. C., Huff, G. S., Cubanski, J. R., Kennedy, A. D. W., McAdam, C. J., McMorran, D. A., Gordon, K. C., & Crowley, J. D. (2015). Comparison of inverse and regular 2-pyridyl-1,2,3-triazole "Click" complexes: Structures, stability, electrochemical, and photophysical properties. *Inorganic Chemistry*, 54, 1572–1587. DOI: 10.1021/ic502557w

[61] Datta, P., Sarkar, D., Mukhopadhyay, A. P., Lopez-Torrez, E., Pastor, C. J., & Sinha, C. (2011). Group-6 metal carbonyl complexes of pyridylbenzoxazole and pyridylbenzothiazole: Synthesis, structure, electrochemistry, photophysical property and DFT calculations. *Journal of Organometallic Chemistry*, 696, 488–495. DOI: 10.1016/j.jorganchem.2010.08.025

[62] Eychenne, R., Guizani, S., Wang, J.- H., Picard, C., Malek, N., Fabre, P.-L., Wolff, M., Machura, B., Saffon, N., Lepareur, N., & Benoist, E. (2017). Rhenium complexes based on an N_2O tridentate click scaffold: From synthesis, structural and theoretical characterization to a radiolabelling study. *European Journal of Inorganic Chemistry*, 69–81. DOI: 10.1002/ejic.201600877

[63] Kim, T. Y., Elliott, A. B. S., Shaffer, K. J., McAdam, C. J., Gordon, K. C., & Crowley, J. D. (2013). Rhenium(I) complexes of readily functionalized bidentate pyridyl-1,2,3-triazole "click" ligands: A systematic synthetic, spectroscopic and computational study. *Polyhedron*, 52, 1391–1398. DOI: 10.1016/j.poly.2012.05.003

[64] Pomp, C., & Wieghardt, K. (1988). Synthesis and reactivity of air-stable $[LRe(NO)(CO)(CH_3)]^+$ (L = 1,4,7-triazacyclononane). Kinetics and mechanism of its reactions with HX (X = Cl, Br, NO_3). Formation of $[\{LRe(NO)(CO)\}_2(\mu\text{-}CH_2OCH_2)]I_2$ containing a bridging 2-oxapropane-1,3-diide. *Inorganic Chemistry*, 27, 3796–3804. DOI: 10.1021/ic00294a025

[65] Laurent, A. D. & Jacquemin, D. (2013). TD-DFT Benchmarks: A Review. *International Journal of Quantum Chemistry*, 113, 2019–2039. DOI: 10.1002/qua.24438

[66] Gierschner, J., Shi, J., Milián-Medina, B., Roca-Sanjuán, D., Varghese, S., & Park, S. Y. (2021). Luminescence in crystalline organic materials: From molecules to molecular solids. *Advanced Optical Materials*, 2002251. DOI: 10.1002/adom.202002251

[67] Ito, S. (2021). Recent advances in mechanochromic luminescence of organic crystalline compounds. *Chemistry Letters*, 50, 649–660. DOI: 10.1246/cl.200874

[68] Einfalt, T., Planinšek, O., & Hrovat, K. (2013). Methods of amorphization and investigation of the amorphous state. *Acta Pharmaceutica*, 63, 305–334. DOI: 10.2478/acph-2013-0026

[69] Carayon, C., Ghodbane, A., Leygue, N., Wang, J., Saffon-Merceron, N., Brown, R., & Fery-Forgues, S. (2019). Mechanofluorochromic Properties of an AIEE-Active 2-Phenylbenzoxazole Derivative: More than Meets the Eye? *ChemPhotoChem*, 3, 545–553. DOI: 10.1002/cptc.201800261

[70] Mu, S., Oniwa, K., Jin, T., Asao, N., Yamashita, M., & Takaishi, S. (2016). A highly emissive distyrylthieno[3,2-*b*]thiophene based red luminescent organic single crystal: Aggregation induced emission, optical waveguide edge emission, and balanced ambipolar carrier transport. *Organic Electronics*, 34, 23–27. DOI: 10.1016/j.orgel.2016.04.001

[71] Fang, H.-H., Yang, J., Feng, J., Yamao, T., Hotta, S., & Sun, H.-B. (2014). Functional organic single crystals for solid-state laser applications. *Laser Photonics Review*, 8, 687–715. DOI: 10.1002/lpor.201300222

[72] Fery-Forgues, S. (2013). Fluorescent organic nanocrystals and non-doped nanoparticles for biological applications. *Nanoscale*, 5, 8428–8442. DOI: 10.1039/C3NR02657D

[73] Mei, J., Huang, Y., & Tian, H. (2018). Progress and trends in AIE-based bioprobes: A brief overview. *ACS Applied Materials & Interfaces*, 10, 12217−12261. DOI: 10.1021/acsami.7b14343